ACADEMIC PRESS

Available online at www.sciencedirect.com

SCIENCE DIRECT®

Journal of Sound and Vibration 264 (2003) 775–794

JOURNAL OF SOUND AND VIBRATION

www.elsevier.com/locate/jsvi

Influence of support properties on the sound radiated from the vibrations of rectangular plates

J. Park[1], L. Mongeau*, T. Siegmund

1077 Ray W. Herrick Laboratories, School of Mechanical Engineering, Purdue University, West Lafayette, IN 47907-1077, USA

Received 27 November 2001; accepted 4 July 2002

Abstract

The control of the forced vibration response of structures through the optimal tuning of its supports is desirable in many applications. Tuning may enhance the dissipation of vibration energy within the supports, thereby reducing fatigue and structure-borne noise. Two different models were developed to calculate the optimal support stiffness that minimizes the velocity response of homogeneous plates. The first model, based on the wave propagation at the edge, yields a good first cut approximation of the optimal properties. The optimal viscous and viscoelastic support stiffness for minimal reflection at the edge was calculated. Maximum absorption of the incident waves occurs when the viscous support stiffness matches the characteristic mechanical impedances of the plate. The second model, based on the Rayleigh–Ritz method, yields more accurate estimates of the optimal support stiffness required to minimize the forced velocity response of the finite rectangular plate. The optimal support properties calculated from the two different methods were in good agreement. This suggested that the modal response of the plate is strongly influenced by the wave reflections at the edges. Finally, the effects of support properties on the sound radiated from the plate were investigated. The optimal support stiffness that minimizes the radiated sound power was found to be smaller than the value that minimizes the velocity response. The results show that both the velocity response and sound radiation are strongly influenced by dissipation of vibration energy at the edges, and demonstrate that support tuning can yield significant noise and vibration reduction.

1. Introduction

Flexible supports affect the modal properties of structures, for example beams and plates. This interaction is utilized in the design of damping treatments through the use of viscoelastic supports.

*Corresponding author. Tel.: +1-765-494-9342; fax: +1-765-494-0787.
E-mail address: mongeau@ecn.purdue.edu (L. Mongeau).
[1] Current address: Structural Acoustics Branch, NASA Langley Research Center, Hampton, VA 23681-2199, USA.

0022-460X/03/$ - see front matter
doi:10.1016/S0022-460X(02)01215-4

Practical applications are seal-supported vehicle side-glass windows. Glass run and belt line seals support side-glass window panels continuously along their edges. The optimization of the seal viscoelastic properties may enhance the sound transmission loss of the windows, and help to reduce interior noise in the vehicle. The approach of optimally tuning the supports is attractive since the mechanical properties of the supports may be easier to modify than the properties of the supported structure itself. Analytical models for the response of the compliantly supported structures are needed to guide design and to calculate the optimal support properties. This problem was the object of the present study.

Many vibration control methods are available for continuous systems. In particular, dynamic absorbers may be used to reduce the vibrations of continuous systems such as rods and beams [1]. Dynamic absorbers consist of a single-degree-of-freedom system (mass, spring, and viscous damper) attached to the primary structure. Optimal values for the absorber natural frequency and damping ratio must be calculated to minimize the vibrations of specific modes at resonance. For plates and shells, the dynamic absorber performance may be analyzed using the receptance method [2]. The presence of the dynamic absorber modifies the modal properties of the primary structure, and must be accounted for.

In cases where structures are compliantly supported, the support mass is often negligible relative to that of the supported structure. The support may be idealized as a stiffness along the boundaries. The effects of support flexibility on the vibration of beams and plates have been investigated before. Kang and Kim [3] investigated the effects of support stiffness on the vibration of beams and plates. The flexible supports were represented by translational and rotational springs with complex stiffnesses. The variation of the modal properties of the structures with the support stiffness was calculated to guide the design of support properties. Macbain and Genin [4] developed numerical methods using a central difference formula to analyze the vibrations of beams with flexible supports. Their method was used to analyze energy dissipation in vibrating Timoshenko beams. The system loss factors were found to increase with a decrease in the support-to-beam elastic modulus ratio. Chen and Zhou [5] investigated the effects of damping on the vibrations of distributed systems using wave propagation methods.

The flow-induced vibration of viscoelastically supported rectangular plates was investigated in Ref. [6]. The case of a homogeneous rectangular plate supported along all four edges by a complex viscoelastic element was treated. The results suggested that there is an optimal support stiffness that minimizes the flow-induced vibration response of the plate.

The object of the current study was to develop theoretical methods to calculate the optimal support stiffness that minimizes the velocity response of the plate, and sound radiation. The effects of compliant viscoelastic supports on the vibro-acoustic properties of a rectangular plate were investigated.

Two different numerical procedures were developed to determine the optimal support properties for minimal vibration response. The wave propagation at the edge was considered first to estimate the optimal stiffness. The compliant supports were idealized as distributed translational and rotational spring and damping elements. Reflection ratios were calculated from the relationship between incident and reflected waves. The stiffness values that minimized the reflection ratios were calculated.

Subsequently, a more detailed model was developed to account for the possible effects of two-dimensional transverse waves. The Rayleigh–Ritz method was used, in conjunction with modified

beam trial functions [6] to calculate the forced vibration response of the viscoelastically supported rectangular plate. This approach ensured fast convergence rates, which is advantageous for the vibration analysis of high order modes. The vibration level in octave bands was calculated as a function of the viscoelastic support properties to determine the optimal stiffness for minimum vibration response. The obtained optimal stiffness values were compared to the previously obtained optimal values for minimal transverse wave reflection. The comparison clarifies the relationship between the modal response of the plate and the condition for optimal vibration energy dissipation at the edges.

Numerical investigations of the sound power radiated from the viscoelastically supported plate were performed to determine the optimal support stiffness for minimal sound radiation. The results were once again compared to the values that minimized the vibration response of the plate. The effects of the support stiffness and vibration energy dissipation on the acoustic properties of the plate were elucidated.

2. Wave propagation at the edge

In the first step of the study, transverse waves approaching normally to the edge were considered. The plate was assumed to be infinitely long in the x direction in order to allow for the calculation of the reflection ratio of the normally incident bending waves. Transverse displacements were assumed to vary only with the distance along the direction normal to the edge, as shown schematically in Fig. 1. The equation of motion for the free transverse vibrations of a homogeneous plate without any constraints in the y direction is [7]

$$D\frac{\partial^4 w}{\partial x^4} + \rho_b h\frac{\partial^2 w}{\partial t^2} = 0, \tag{1}$$

where $D = Eh^3/12(1-v^2)$ is the bending stiffness, w is the transverse displacement, ρ_b is the density, h is the thickness, E is Young's modulus, and v is the Poisson's ratio. Two boundary conditions at the edge are

$$D\frac{\partial^3 \hat{w}(0)}{\partial x^3} = -\hat{S}_t \hat{w}(0), \tag{2a}$$

$$D\frac{\partial^2 \hat{w}(0)}{\partial x^2} = \hat{S}_r \frac{\partial \hat{w}(0)}{\partial x}, \tag{2b}$$

where $\hat{S}_t$ and $\hat{S}_r$ are the complex translational and rotational boundary stiffnesses, respectively. The usual complex notation is used, $w(x,t) = \mathrm{Re}\{\hat{w}(x)e^{i\omega t}\}$. To calculate the reflection ratio at the edge, normally incident harmonic bending waves with complex amplitude $\hat{B}$ were assumed to propagate toward the edge from $x = \infty$. A similar approach was used by Chen and Zhou [5] to calculate asymptotic estimates for the reflection ratios. The plate displacement at the edge is expressed as

$$\hat{w}(x) = \hat{A}e^{-ik_b x} + \hat{B}e^{ik_b x} + \hat{C}e^{-k_b x}, \tag{3}$$

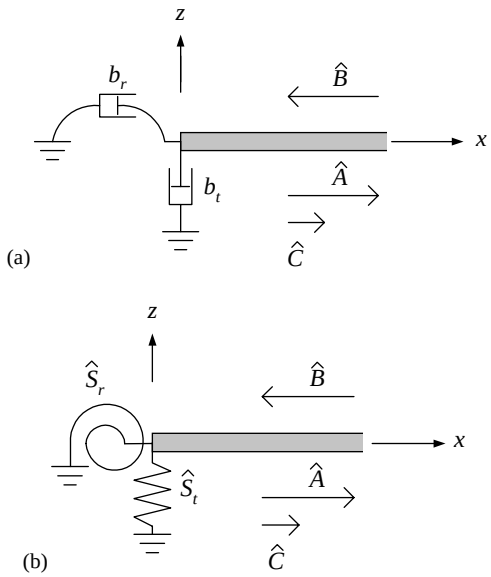

Fig. 1. Normally, incident and reflected bending waves at the edge of a plate. (a) viscous support; (b) viscoelastic support.

where $\hat{A}$ and $\hat{C}$ are the complex amplitudes of the reflected harmonic wave and the exponentially decaying wave, respectively, and k_b is the wave number related to the circular frequency, $k_b = \left(\omega^2\rho_b h/D\right)^{1/4}$.

Applying the boundary conditions shown in Eq. (2), the transfer functions between the incident and reflected harmonic waves are

$$\frac{\hat{A}}{\hat{B}} = \frac{(\mathrm{i}+1) + 2\mathrm{i}\hat{R} - 2\hat{T} - (\mathrm{i}+1)\hat{R}\hat{T}}{(\mathrm{i}-1) + 2\mathrm{i}\hat{R} + 2\hat{T} - (\mathrm{i}-1)\hat{R}\hat{T}}, \tag{4a}$$

$$\frac{\hat{C}}{\hat{B}} = \frac{2\mathrm{i}\left(1 + \hat{R}\hat{T}\right)}{(\mathrm{i}-1) + 2\mathrm{i}\hat{R} + 2\hat{T} - (\mathrm{i}-1)\hat{R}\hat{T}}, \tag{4b}$$

where the non-dimensional stiffness parameters are defined as

$$\hat{T} = \frac{\hat{S}_t}{Dk_b^3}, \tag{5a}$$

$$\hat{R} = \frac{\hat{S}_r}{Dk_b} \tag{5b}$$

To study the dissipation of vibrational energy at the edge, two different boundary conditions, viscous and viscoelastic boundaries, were considered. Note that when the plate is supported elastically, the boundary stiffness is purely real and the magnitude of the reflected waves, $|\hat{A}|$, is the same as that of the incident waves, $|\hat{B}|$. This shows that there is no energy dissipation at the edge of the elastically supported plate.

2.1. Viscous supports

When the plate is supported viscously, Fig. 1(a), the non-dimensional stiffness parameters are given as

$$\hat{T} = \frac{\mathrm{i}\omega b_t}{Dk_b^3} \tag{6a}$$

$$\hat{R} = \frac{\mathrm{i}\omega b_r}{Dk_b} \tag{6b}$$

From Eqs. (4) and (6), complete absorption of incident waves occurs when the damping coefficients are

$$b_t = \frac{Dk_b^3}{\omega}, \tag{7a}$$

$$b_r = \frac{Dk_b}{\omega}. \tag{7b}$$

These viscous damping coefficients are identical to the characteristic translational and rotational mechanical impedances of the transversely vibrating plate, which are defined as

$$\frac{Q_{xz}}{\dot{w}} = \frac{Dk_b^3}{\omega}, \tag{8a}$$

$$\frac{M_{xx}}{\dot{\varphi}} = \frac{Dk_b}{\omega}, \tag{8b}$$

where $Q_{xz} = D\partial^3 w/\partial x^3$ is the shear force, $M_{xx} = D\partial^2 w/\partial x^2$ is the bending moment, and φ_x is the angular deflection. The characteristic mechanical impedances in Eq. (8) were calculated by considering harmonic bending waves propagating in the negative x-direction such that the plate displacement is given as $w(x,t) = \mathrm{Re}\{\hat{B}\mathrm{e}^{\mathrm{i}(\omega t + kx)}\}$. Complete absorption of the incident waves at the boundary occurs when the boundary impedances match the characteristic mechanical impedances. The plate supports must include both translational and rotational viscous damping elements to completely absorb the incident waves. In contrast with the characteristic mechanical impedance of vibrating strings, which is frequency independent [5], the characteristic translational and rotational impedances of transversely vibrating plates depend on frequency. Thus, the optimal support properties also depend on frequency.

2.2. Viscoelastic supports

For viscoelastically supported plates, Fig. 1(b), the restraints from the supports may be idealized by a combination of complex translational and rotational springs. In this case, the non-dimensional boundary stiffnesses are given by

$$\hat{T} = T(1 + \mathrm{i}\eta_t) = \frac{S_t}{Dk_b^3}(1 + \mathrm{i}\eta_t), \tag{9a}$$

$$\hat{R} = R(1 + \mathrm{i}\eta_r) = \frac{S_r}{Dk_b}(1 + \mathrm{i}\eta_r), \tag{9b}$$

where S_t and S_r are the real parts of the complex support stiffnesses, and η_t and η_r are the loss factors. By substituting Eq. (9) into Eq. (4), the reflection ratios were calculated in terms of T, R, η_t, and η_r. When the real part of the complex support stiffnesses, S_t and S_r, and the wavenumber are non-zero, the reflection ratio, $|\hat{C}/\hat{B}|$, is always positive. This shows that a complete dissipation of the incident waves may not always be possible for viscoelastically supported plates. However, a support stiffness that minimizes the amplitude of reflected harmonic bending waves may be found. The exponentially decaying waves with complex amplitudes, $\hat{C}$, have a limited influence, and only at the edges. They were neglected in the calculation. Only the reflected propagating waves with complex amplitudes, $\hat{A}$, are minimized in the optimization problem. The minimum reflection occurs when the parameters of the boundary stiffnesses satisfy the equations:

$$\frac{\partial|\hat{A}/\hat{B}|^2}{\partial T}=0, \tag{10a}$$

$$\frac{\partial|\hat{A}/\hat{B}|^2}{\partial R}=0, \tag{10b}$$

$$\frac{\partial|\hat{A}/\hat{B}|^2}{\partial \eta_t}=0, \tag{10c}$$

$$\frac{\partial|\hat{A}/\hat{B}|^2}{\partial \eta_r}=0. \tag{10d}$$

The Hessian matrix [8] was calculated to determine whether the roots correspond to a minimum, a maximum, or a saddle point. Values that satisfy Eq. (10) must be positive to be physically acceptable. From Eqs. (10) and (4a), four equations were obtained to calculate the optimal support stiffness for minimum reflection:

$$\begin{aligned} a_{1t}\left[2\eta_t+2a_{3t}R+a_{2t}R^2+a_{1r}\eta_t(4+a_{1r}R)R^3\right]T^2+2a_{1t}\eta_r R\left(1-a_{1r}R^2\right)T \\ -\left[\eta_t(1+4R)+a_{2t}R^2+2a_{1r}R^3\left(a_{3t}+\eta_t a_{1r}R\right)\right]=0, \end{aligned} \tag{11a}$$

$$\begin{aligned} a_{1r}\left[2\eta_r-2a_{3r}T+a_{2r}T^2-a_{1t}\eta_r(4-a_{1t}T)T^3\right]R^2+2a_{1r}\eta_t T\left(1-a_{1t}T^2\right)R \\ -\left[\eta_r(1-4T)+a_{2r}T^2-2a_{1t}T^3\left(a_{3r}-\eta_r a_{1t}T\right)\right]=0, \end{aligned} \tag{11b}$$

$$\begin{aligned} &T\left\{T^2\left[2+6R+a_{4r}R^2+a_{1r}R^3(4+a_{1r}R)\right]\eta_t^2\right. \\ &+2\eta_r TR\left[1-a_{1r}R^2-2T(1+R)\right]\eta_t-a_{4r}R^2\left(T^2+1\right) \\ &+TR(6+8R-6T)-\left(1-2T+4R+2T^2\right) \\ &\left.-a_{1r}R^3\left(6-6T+4T^2\right)-a_{1r}^2R^4\left(2-2T+T^2\right)\right\}=0, \end{aligned} \tag{11c}$$

$$\begin{aligned} &R\left\{R^2\left[2-6T+a_{4t}T^2+a_{1t}T^3(a_{1t}T-4)\right]\eta_r^2\right. \\ &+2\eta_T TR\left(1-a_{1t}T^2+2R(1-T)\right)\eta_r-a_{4t}T^2\left(R^2+1\right) \\ &+TR(6+6R-8T)-\left(1+2R-4T+2R^2\right) \\ &\left.+a_{1f}T^3\left(6+6R+4R^2\right)-a_{1t}^2T^4\left(2+2R+R^2\right)\right\}=0, \end{aligned} \tag{11d}$$

where

$$a_{1t} = 1 + \eta_t^2, \quad a_{1r} = 1 + \eta_r^2, \quad a_{2t} = \eta_r^2\eta_t + 7\eta_t - 2\eta_r, \quad a_{2r} = \eta_t^2\eta_r + 7\eta_r - 2\eta_t,$$
$$a_{3t} = 3\eta_t - \eta_r, \quad a_{3r} = 3\eta_r - \eta_t, \quad a_{4t} = 7 + \eta_t^2, \quad a_{4r} = 7 + \eta_r^2.$$

The Newton–Rapson method was used to solve Eq. (11) numerically. The solution of Eq. (11) is not unique, i.e., there are multiple solutions that yield the same absolute minimum value of zero. Three different special cases were investigated.

2.2.1. Plate supported by translational viscoelastic elements

Consider the plate supported by translational springs only ($R=0$). The effects of the translational stiffness on the reflection ratio, $\left|\hat{A}/\hat{B}\right|^2$, are shown in Fig. 2(a) for various values of η_t. In this case (for $R=0$), the real part and the loss factor of the optimal translational stiffness for minimum reflection of propagating waves from the boundary are, from Eqs. (11a) and (11c),

$$S_{t,opt} = \tfrac{1}{2}k_b^3 D, \tag{12a}$$

$$\eta_{t,opt} = 1. \tag{12b}$$

The corresponding minimum reflection ratio is zero. The value of the loss factor in Eq. (12) is greater than typical loss factor values for many viscoelastic materials, which are usually less than 0.3 [9]. For the loss factor fixed to a value smaller than unity, the optimal support stiffness for minimal reflection is, from Eq. (11a),

$$S_{t,opt} = \frac{k_b^3 D}{\sqrt{2\left(1+\eta_t^2\right)}}. \tag{13}$$

In many applications, it may be far more convenient to vary the real stiffness, S_t and S_r, by changing the geometry of the support, the material thickness, the contact area, and/or the curvature than to change the loss factor which depends mostly on the support material. Equation (13) should then be used to approximately estimate the optimal support stiffness.

2.2.2. Plate supported by rotational viscoelastic elements

Fig. 2(b) shows the effects of the rotational stiffness for $T=0$. The real part and the loss factor of the optimal rotational stiffness for minimum reflection of propagating bending waves from the boundary are, from Eq. (11b),

$$S_{r,opt} = -\tfrac{1}{2}k_b D, \tag{14a}$$

$$\eta_{r,opt} = 1. \tag{14b}$$

In the above calculated optimal values, the rotational stiffness should be negative which was not realistic in this case. As shown in Fig. 2(b), there are no conditions for complete suppression of the reflected waves if the rotational stiffness is positive. When the loss factor of the rotational element is smaller than unity the optimal support stiffness for minimum bending wave reflection

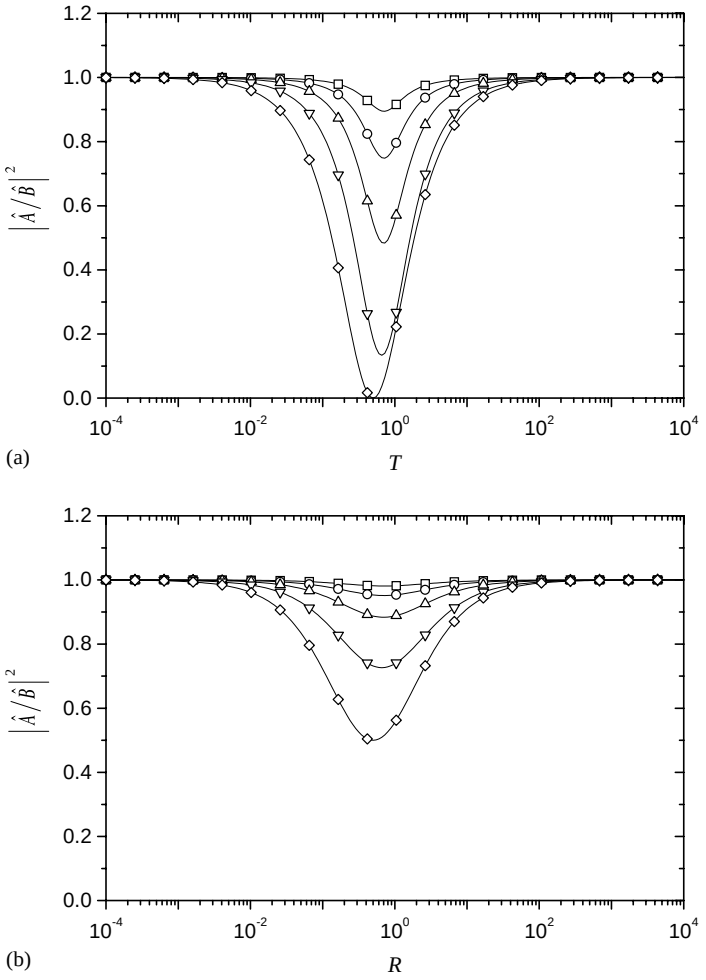

Fig. 2. Reflection ratio, $|\hat{A}/\hat{B}|$, versus non-dimensional stiffness parameters. (a) Effects of translational stiffness for $R=0$; (b) effects of rotational stiffness for $T=0$. Loss factors, η_t and η_r: —□—, 0.023 —○—, 0.06; —▽—, 0.15 —△—, 0.4 —◇—, 1.

is, from Eq. (11b),

$$S_{r,opt} = \frac{k_b D}{\sqrt{2(1+\eta_r^2)}}. \tag{15}$$

A comparison between Fig. 2(a) and (b) shows that the minimum reflection ratio is lower for the translational springs than it is for the rotational springs for the same value of the loss factor. This result suggests that the restriction of the translational motion is more effective than the restriction of the rotational motion to increase the dissipation of vibration energy at the boundary. The effects of the translational stiffness on the flow-induced vibrations of viscoelastically supported plates were also discussed in Ref. [6].

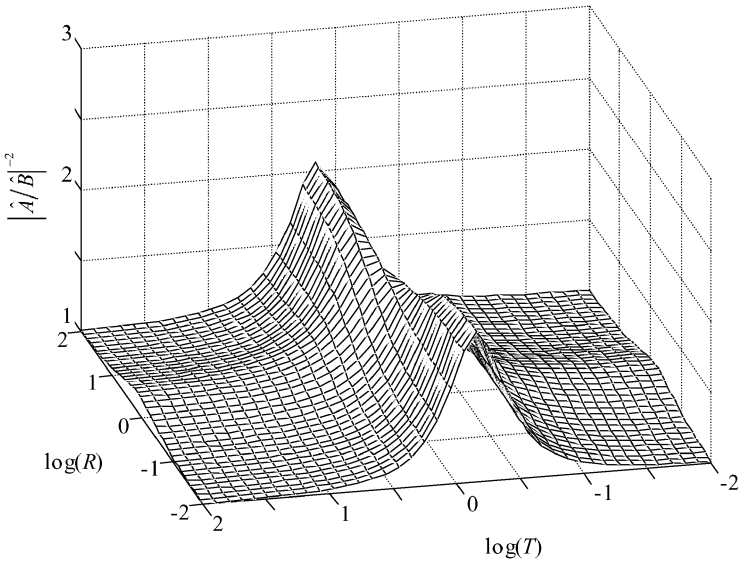

Fig. 3. Effects of the non-dimensional stiffness parameters on the inverse reflection ratio. $\eta_t = \eta_r = 0.15$.

2.2.3. Plate supported by both translational and rotational viscoelastic elements

If the plate is supported by both translational and rotational stiffnesses, the optimal support stiffness is different from the values for each element type alone, reported in Sections 2.2.1. and 2.2.2. A fixed loss factor value was imposed in this case. As per the discussion in Section 2.2.1, this value was chosen to be smaller than unity. Fig. 3 shows the effects of the support properties on the reflection ratio for $\eta_t = \eta_r = 0.15$. The inverse of the reflection ratio is plotted for visualization purposes. The values that satisfy Eqs. (11a) and (11b) include a saddle point for $T = 0.989$ and $R = 0.989$. The saddle point migrates towards decreasing values of T and R as the loss factors are increased. Two extrema are found at the boundaries, $R = 0$ and ∞ (the graph shows only a limited range for R). As $R \to 0$, the optimal translational stiffness is the value calculated from Eq. (13). As $R \to \infty$, the optimal translational stiffness is twice the value calculated from Eq. (13). The minimum reflection ratios are the same for both extrema. This suggests that both extrema are absolute minima. These trends are the same for different values of η_t and η_r.

The effects of the finite size of the plate, and the associated two-dimensional modal structural response may well influence the optimal stiffness values. In the following sections, a different approach was followed to calculate these values numerically.

3. Forced vibration of the rectangular viscoelastically supported plate

Fig. 4(a) illustrates one possible example of sound radiation from forced vibrations of a viscoelastically supported plate. This configuration is intended to idealize a seal-supported vehicle side-glass window. Fig. 4(b) shows a schematic of the viscoelastically supported rectangular plate.

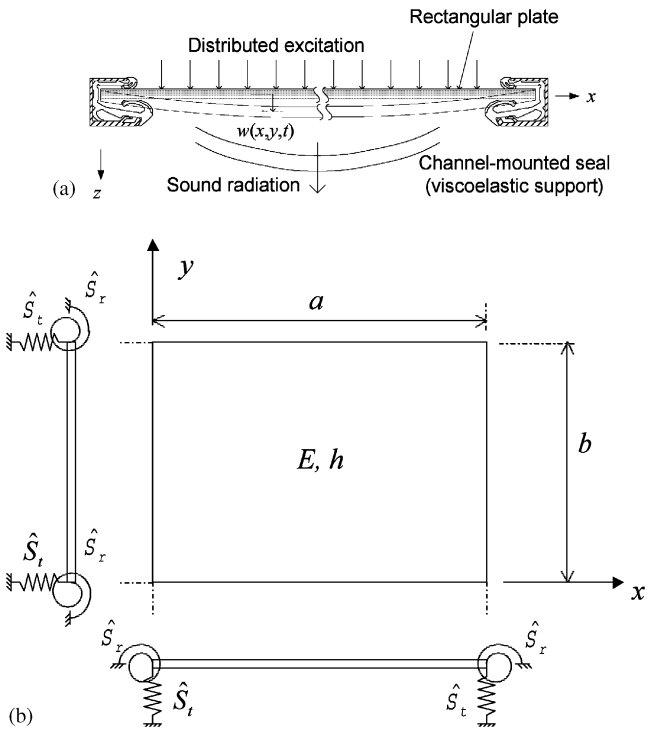

Fig. 4. (a) Sound radiation from forced vibrations of a seal-supported rectangular plate. (b) Geometry of the rectangular plate and its boundary conditions. The supports are shown from a side view of the plate.

The plate has uniform thickness h, and dimensions $a \times b$. The motion of the four edges was assumed to be restrained by translational and rotational springs with complex stiffnesses, $\hat{S}_t$ and $\hat{S}_r$, respectively.

In general, many applications require the calculation of the response of the structure to randomly distributed excitations. In this study, a simplified model for the distributed excitation, based on delta functions, was used. When the excitation over the plate is perfectly incoherent, homogeneous, and stationary, the cross-spectral density of the distributed excitations between two locations, $\mathbf{s}_1$ and $\mathbf{s}_2$, is given by [10]

$$G_{pp}(\mathbf{s}_1, \mathbf{s}_2, \omega) = \Phi_p(\omega)\delta(\mathbf{s}_1 - \mathbf{s}_2), \tag{16}$$

where Φ_p is the pressure spectral density. To calculate the forced vibration response, the frequency transfer function between a harmonic excitation at one location and the resulting harmonic transverse displacement response at another location was used. The frequency transfer function between one applied point force at $\mathbf{s}_1$ and the associated velocity response at $\mathbf{s}_2$ is [10]

$$H(\mathbf{s}_1, \mathbf{s}_2, t) = \sum_{j=1}^{N^2} \hat{\Psi}_j^*(\mathbf{s}_1)\hat{\Psi}_j(\mathbf{s}_2)\hat{H}_j(\omega) \tag{17}$$

Here, $\hat{\Psi}_j$ are the modal shape functions and $\hat{H}_j$ are the frequency response functions for the generalized co-ordinates, given as

$$\hat{H}_j(\omega) = \frac{1}{\rho_b hab\left(-\omega^2 + \hat{\omega}_j^2\right)}, \tag{18}$$

where $\hat{\omega}_j (= \omega_{nj}\sqrt{1+\mathrm{i}\eta_j})$ are the natural frequencies. The Rayleigh–Ritz method was used applying beam functions as the trial functions to calculate the modal shape functions and the natural frequencies. The plate vibration response was approximated as an N^2-degrees-of-freedom discrete system. Details of the Rayleigh–Ritz method used in this study are described in Ref [6]. The modal shape functions, $\hat{\Psi}_j$, were orthogonal, i.e.,

$$\int_0^a \int_0^b \hat{\Psi}_j(x,y)\hat{\Psi}_m^*(x,y)\,\mathrm{d}x\,\mathrm{d}y = (ab)\delta_{jm}. \tag{19}$$

The spatially averaged mean square velocity of the plate, v_{av}, is then [10]

$$v_{av} = \sum_{j=1}^{N^2}\left|\omega\hat{H}_j(\omega)\right|^2 \int_S\int_S \hat{\Psi}_j(\mathbf{s}_1)\hat{\Psi}_j^*(\mathbf{s}_2)G_{pp}(\mathbf{s}_1,\mathbf{s}_2,\omega)\mathrm{d}\mathbf{s}_1\mathrm{d}\mathbf{s}_2, \tag{20}$$

where S is the plate surface. When delta functions are used as the correlation functions, Eq. (16), the spatial average of the mean square velocity is

$$v_{av} = ab\Phi_p(\omega)\sum_{j=1}^{N^2}\left|\omega\hat{H}_j(\omega)\right|^2. \tag{21}$$

In the numerical simulations performed in this study, it was assumed that the wall pressure spectral density (Φ_p) is unity over the entire frequency range of interest. The spatially averaged mean square velocity in octave bands, with center, lower, and upper frequency limits of ω_0, ω_1, and ω_2, respectively, was calculated analytically using

$$v_{\omega_0} = \frac{1}{2ab\left(\rho_b h\right)^2}\sum_{j=1}^{N^2}\frac{1}{\omega_{nj}^2\eta_j}\mathrm{Im}\left\{\hat{\omega}_j \ln\frac{\left(\hat{\omega}_j-\omega_1\right)\left(\hat{\omega}_j+\omega_2\right)}{\left(\hat{\omega}_j+\omega_1\right)\left(\hat{\omega}_j-\omega_2\right)}\right\}. \tag{22}$$

4. Sound radiation

4.1. Sound radiation from a viscoelastically supported plate

To predict the effects of support properties on the sound radiated from the plate, the radiated sound power is calculated. Fig. 5 shows the co-ordinate system used in the estimation of the radiated sound power. Assuming a baffled plate mounted on an infinite rigid plane surface, the farfield complex acoustic pressure was calculated using the Rayleigh integral [7]

$$\hat{p}(r,\theta,\phi) = -\rho_a\omega^2\frac{\mathrm{e}^{-\mathrm{i}k_a r}}{2\pi r}\int_0^a\int_0^b \hat{w}(x,y)\mathrm{e}^{\mathrm{i}k_a(x\sin\theta\cos\phi + y\sin\theta\sin\phi)}\mathrm{d}x\mathrm{d}y, \tag{23}$$

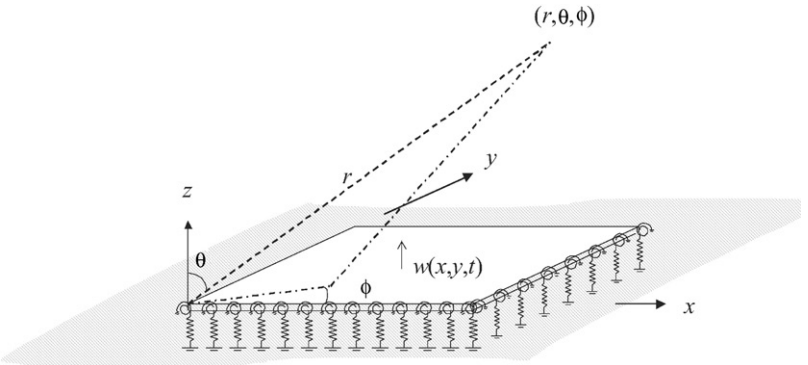

Fig. 5. Co-ordinate systems to calculate the radiated sound power from the baffled and viscoelastically supported plate.

where k_a is the wave number ($k_a = \omega / c$) with c the speed of sound in air and ρ_a is the density of air. The farfield assumption requires r to be much larger than the plate dimensions, a and b. Accordingly, the radiated sound power, W_r, was calculated as the integral of the farfield acoustic intensity over a hemisphere surrounding the plate as follows [11]:

$$W_r = \frac{1}{2}\int_0^{2\pi}\int_0^{\pi/2} \frac{1}{\rho_a c}|\hat{p}|^2 r^2 \sin\theta \, \mathrm{d}\theta \, \mathrm{d}\phi. \tag{24}$$

By substituting Eq. (23) into Eq. (24), the sound power is

$$W_r = \frac{\rho_a \omega^4}{8\pi^2 c}\int_0^{2\pi}\int_0^{\pi/2}\int_S\int_S \hat{G}_{yy}(\mathbf{r}_1, \mathbf{r}_2, \omega) \mathrm{e}^{\mathrm{i}k_a(\mathbf{r}_2 - \mathbf{r}_1)\cdot(\sin\theta\cos\phi,\, \sin\theta\sin\phi)} \, \mathrm{d}\mathbf{r}_1 \mathrm{d}\mathbf{r}_2 \sin\theta \, \mathrm{d}\theta \, \mathrm{d}\phi, \tag{25}$$

where $\hat{G}_{yy}$ is the cross-spectral density of the plate displacements between two locations, $\mathbf{r}_1$ and $\mathbf{r}_2$, given by

$$\hat{G}_{yy}(\mathbf{r}_1, \mathbf{r}_2, \omega) = \sum_{m=1}^{N^2}\sum_{n=1}^{N^2}\int_S\int_S \hat{\Psi}_n^*(\mathbf{r}_1)\hat{\Psi}_n(\mathbf{s}_1)\hat{\Psi}_m(\mathbf{r}_2)\hat{\Psi}_m^*(\mathbf{s}_2)\hat{H}_n^*(\omega)\hat{H}_m(\omega)G_{pp}(\mathbf{s}_1, \mathbf{s}_2, \omega) \, \mathrm{d}\mathbf{s}_1 \mathrm{d}\mathbf{s}_2. \tag{26}$$

In Eq. (25), the contributions of the intermodal terms are accounted for. If the correlation function of the distributed pressure is idealized as a delta function, Eq. (16), the intermodal terms disappear, and the radiated sound power expression is simplified, i.e.,

$$W_r = \frac{ab\rho_a\omega^4\Phi_p(\omega)}{8\pi^2 c}\sum_{j=1}^{N^2}\left|\hat{H}_j(\omega)\right|^2 \int_0^{2\pi}\int_0^{\pi/2}\left|\int_S \hat{\Psi}_j(\mathbf{s}_1)\, \mathrm{e}^{\mathrm{i}k_a\mathbf{s}_1\cdot(\sin\theta\cos\phi,\, \sin\theta\sin\phi)} \, \mathrm{d}\mathbf{s}_1\right|^2 \sin\theta \, \mathrm{d}\theta \, \mathrm{d}\phi. \tag{27}$$

The radiation efficiency is widely used to estimate the sound power radiated from vibrating structures. From the farfield sound intensity, Wallace [12] derived approximate expressions for the radiation efficiency of a simply supported, baffled plate. Berry et al. [11] calculated the radiation efficiency of plates with general boundary conditions. In the present study, the radiation efficiency of the jth mode, σ_j, was calculated using

$$\sigma_j = \frac{k_a^2}{4\pi^2 ab}\int_0^{2\pi}\int_0^{\pi/2}\left|\int_S \hat{\Psi}_j(\mathbf{s}_1)\mathrm{e}^{\mathrm{i}k\mathbf{s}_1\cdot(\sin\theta\cos\phi,\, \sin\theta\sin\phi)}\mathrm{d}\mathbf{s}_1\right|^2 \sin\theta \mathrm{d}\theta\mathrm{d}\phi. \tag{28}$$

From Eqs. (27) and (28), the radiated sound power is

$$W_r = \frac{\rho_a c \Phi_p(\omega)}{2} \sum_{j=1}^{N^2} \sigma_j \left| \frac{\omega}{\rho_b h\left(-\omega^2 + \hat{\omega}_j^2\right)} \right|^2. \tag{29}$$

To calculate the radiation efficiency, the integration with respect to θ and ϕ was performed using Simpson's 3/8 rule: the integral domain (θ, ϕ) was sub-divided into 40×40 equally spaced elements.

5. Numerical results and discussions

5.1. Effects of support stiffness on vibration response

For the Rayleigh–Ritz method predictions, the plate was approximated as a system with 196 degrees of freedom ($N = 14$). The plate properties were chosen to be: $a = 0.466$ m; $= 0.375$ m; $h = 0.00338$ m; $\rho_b = 2700$ kg/m^3; $E = 7.2 \times 10^{10}$ Pa; and $v = 0.34$. Fig. 6 shows the spatially averaged mean square velocity calculated from Eq. (21) as a function of the support stiffnesses, S_t for $\eta_t = 0.15$ and $S_r = 0$. The calculated natural frequencies change from those of a freely supported plate to those of a simply supported plate as S_t is increased. A minimum in the velocity response, for a fixed excitation amplitude, may be identified between the two limits.

Fig. 7 shows the spatially averaged mean square velocity in octave bands calculated from Eq. (22) as a function of the translational stiffness, S_t for $\eta_t = 0.15$ and $S_r = 0$. The results for

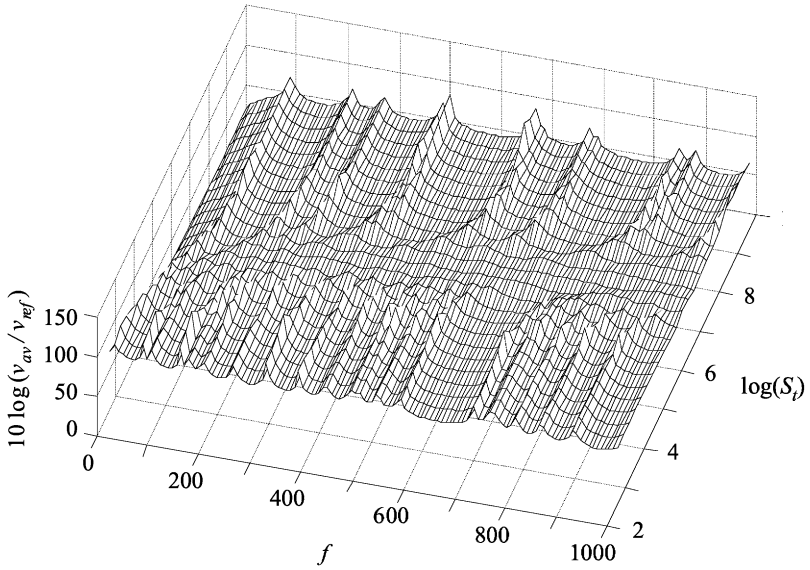

Fig. 6. Frequency dependence of the spatially averaged mean square velocity versus translational stiffness. $\hat{S}_t = S_t(1 + 0.15\mathrm{i})$ and $\hat{S}_r = 0$.

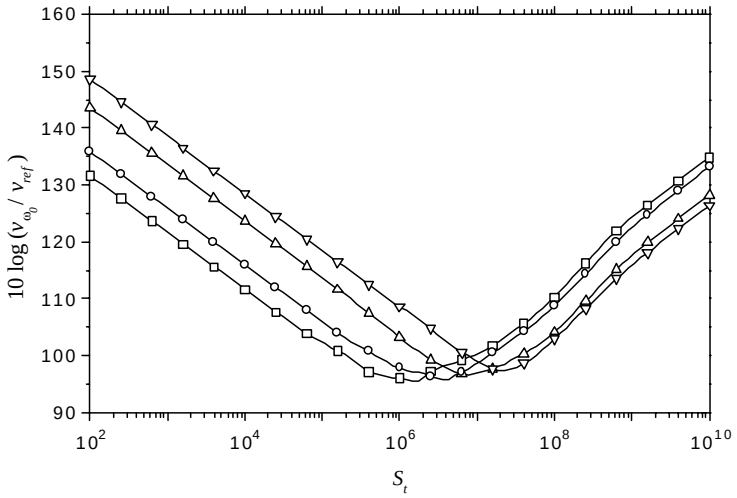

Fig. 7. Effects of the translational stiffness on spatially averaged velocity level in octave bands. $\hat{S}_t = S_t\,(1+0.15\mathrm{i})$ and $\hat{S}_r = 0$. Center frequencies: —□—, 250 Hz; —○—, 500 Hz; —△—, 1000 Hz; —▽—, 2000 Hz.

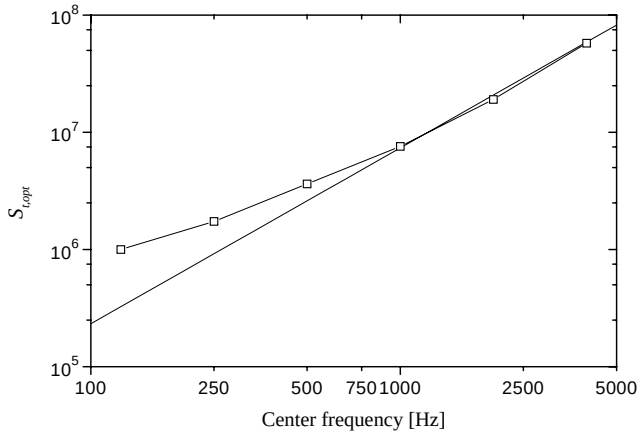

Fig. 8. Optimal translational stiffness calculated from the condition of: ——, minimum reflections from the edge; —□—, minimum spatially averaged mean square velocity.

octave bands centered at 250, 500, 1000, and 2000 Hz are shown. For each octave band, there is an absolute minimum in the calculated velocity. The optimal translational stiffness that minimized the vibration response was determined from the simulation results for each octave band, and is shown in Fig. 8 together with the translational stiffness calculated from Eq. (13). The calculated optimal translational stiffnesses are generally in good agreement, which indicates that Eq. (13) is a good first cut model to determine the optimal support properties. The finite size of the plate and the modal response caused the differences between the two predictions. This difference increases when the modal density (the average number of modes per unit frequency band) is small. For

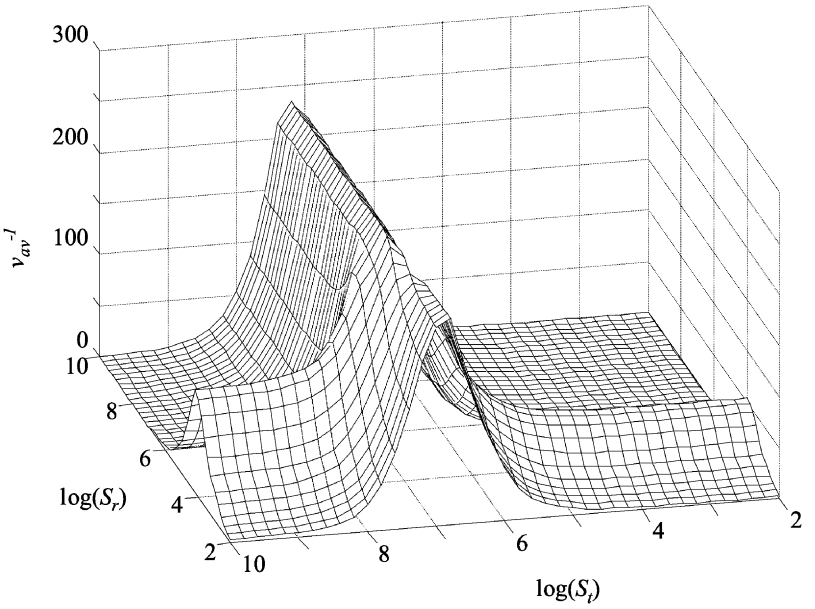

Fig. 9. Effects of translational and rotational stiffness on spatially averaged mean square velocity in the 1000 Hz octave band, $\eta_t = \eta_r = 0.15$.

homogeneous, rectangular plates, the modal density may be calculated using [13]

$$n(f) = \sqrt{\frac{3\rho_b}{E}}\frac{ab}{h}. \tag{30}$$

The modal density is independent of frequency. Eq. (30) yields a value of 0.017 modes/Hz for the plate mechanical properties used in this study. The bandwidth of octave bands increases as the center frequency is increased. Consequently, the high-frequency octave bands include a larger number of modes causing the two predictions, i.e., the numerically predicted optimal stiffness and the values from Eq. (13), to agree well with each other. This is the case indeed for the results for the 1000 and 2000 Hz octave bands in Fig. 8.

Fig. 9 shows the predicted vibration response of the plate supported by both translational and rotational springs. The inverse of the mean square velocity is plotted, to enhance the contrast between the main trends. The trends are very similar to those observed in the calculated reflection ratios shown in Fig. 3, except that the absolute minimum value of the vibration response occurred not on the boundaries but when the translational and rotational stiffnesses were both close to twice the values calculated from Eqs. (13) and (15), respectively. This result is due to the contributions of the modal response of the plate.

To investigate the effects the modal response, the optimal stiffness was calculated for various values of the plate aspect ratio, a/b. The plate dimension, a, remained the same and only the dimension, b, was varied to change the aspect ratio. Fig. 10 shows the simulation results: the optimum stiffness calculated from Eq. (13) and the values that minimize the forced velocity response for the 500,1000 and 2000 Hz octave bands. The difference between the two predictions

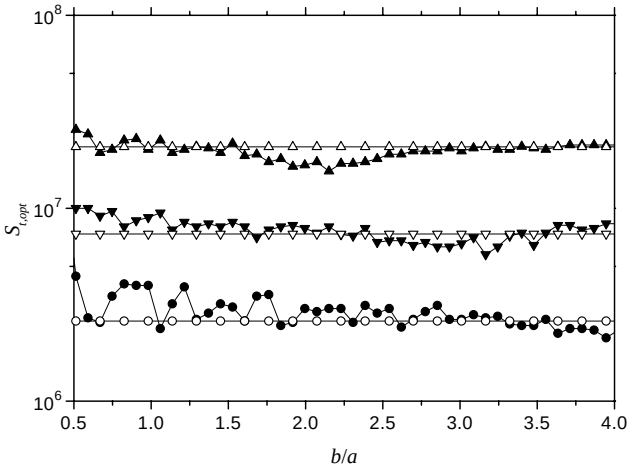

Fig. 10. Effects of the plate aspect ratio (b/a) on the optimal translational stiffness. $\hat{S}_t = S_t\ (1+0.15\mathrm{i})$ and $\hat{S}_r = 0$. Minimum reflections from the edge, center frequencies: —○—, 500 Hz; —▽—, 1000 Hz; —△—, 2000 Hz.Minimum spatially averaged mean square velocity, center frequencies: —●—, 500 Hz; —▼—, 1000 Hz; —▲—, 2000 Hz.

is due to the modal response of the plate as manifested by the change in the natural frequencies with the plate aspect ratio. As shown in Fig. 10, the predicted optimal stiffness from Eq. (13) can be greater or smaller than the optimal stiffness that minimizes the forced vibration response. Aside from these minor variations, the optimal translational stiffnesses that minimize the forced velocity response are in good agreement with the values calculated from Eq. (13).

5.2. *Effects of support stiffness on the radiated sound*

The effects of the support properties on the radiated sound were also investigated. Fig. 11 shows the radiation efficiency of the 1st, 2nd, and 4th modes calculated using Eq. (28) for three different translational stiffness values. For $S_t = 10^{10}$ Pa, the calculated radiation efficiencies agree well to those of the simply supported plate calculated using the approximate formula presented in reference [12]. For $S_t = 10^2$ Pa, the plate response is similar to that of a free plate. As shown in Fig. 11, the radiation efficiency depends more strongly on the mode number than on the boundary stiffness. Similar trends for the dependence of the calculated radiation efficiency on the boundary conditions were reported in Ref. [11].

The sound power radiated from the plate, calculated using Eq. (29), is shown as a function of the translational stiffness in Fig 12. For $S_t = 10^2$ Pa, the plate response is analogous to that of a free plate. In this case, sound is radiated mostly by the "piston mode" of vibration [11]. Most other low-frequency modes of resonance did not contribute significantly to the calculated sound power. For this reason, free plates are inefficient radiators of sound compared to simply supported plates.

Fig. 13 shows the octave band sound power calculated from numerical integration of Eq. (29) with respect to frequency using $\Delta f = 1$ Hz.Due to the numerical integration, the variation of the octave band sound power with the translational stiffness is less smooth than that of the velocity

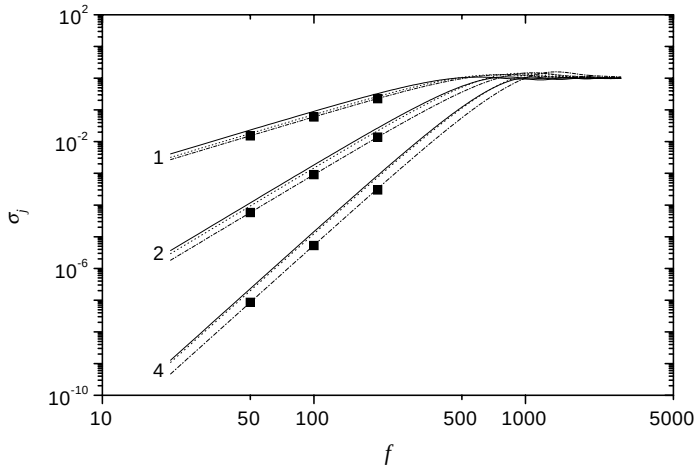

Fig. 11. Radiation efficiency of 1st, 2nd, 4th resonance modes of the plate supported by the translational stiffness only. $\eta_t = 0.15$, S_t: ——, 10^2 Pa; ——-, 10^6 Pa; - - - - -, 10^{10} Pa. The radiation efficiency of the simply supported plate predicted using the approximate formula by Wallace (1971) is shown as keys (■).

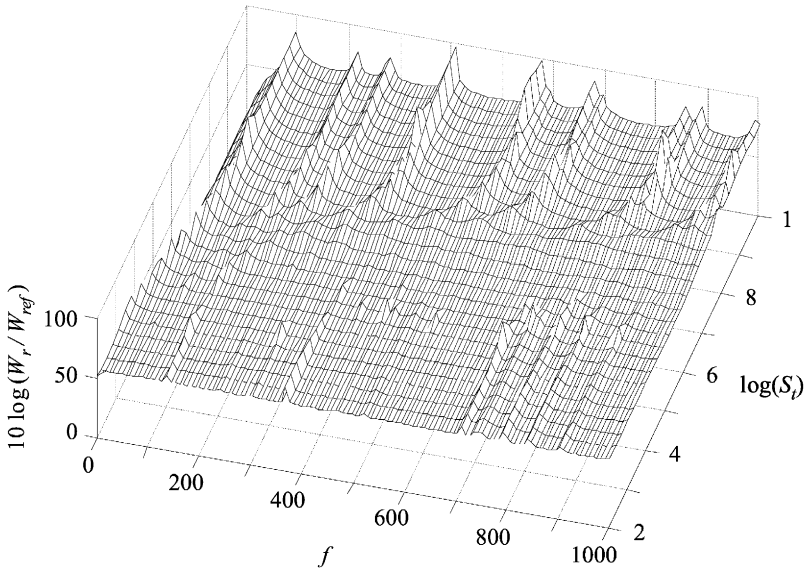

Fig. 12. Frequency dependence of the sound power radiated from the plate vs. translational stiffness. $\hat{S}_t = S_t\,(1 + 0.15\mathrm{i})$ and $\hat{S}_r = 0$.

response in Fig. 7. For each octave band, there is an optimal support stiffness that minimizes the sound radiation. The optimal stiffness again increases with the center frequency. The boundary stiffness increases the natural frequencies of the system, as shown in Fig. 6, which results in increased radiating wave number components [7]. To minimize the radiating wave number

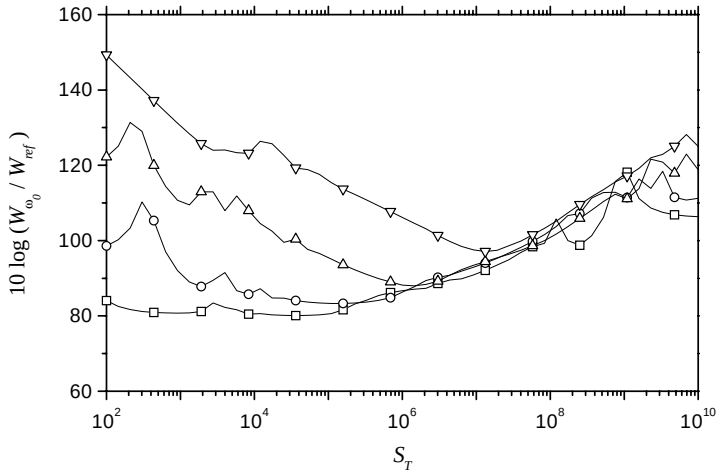

Fig. 13. Effects of the translational stiffness on radiated sound power in octave bands. $\hat{S}_t = S_t\,(1+0.15\mathrm{i})$ and $\hat{S}_r = 0$. Center frequencies: —□—, 250 Hz; —○—, 500 Hz; —△—, 1000 Hz; —▽—, 2000 Hz.

components, the translational stiffness should be as small as possible. When the translational stiffness is too small, however, the velocity response increases. Consequently, the optimal translational stiffnesses for minimal sound radiation are lower than the optimal values for minimal velocity response. The difference between the two optimal values decreases as the center frequency increases. This may need to be taken into consideration in practical applications, such as side-glass vehicle windows, where control of the radiated sound is the primary objective.

6. Conclusions

The effects of the support properties on the forced vibration response and the associated radiated sound of viscoelastically supported rectangular plates were investigated. Approximate relations based on wave propagation at the edge were first derived. These allowed the calculation of reflection ratios from which the optimal stiffness for maximum absorption of incident transverse waves was determined. The optimal properties of translational and rotational viscous dampers were found to coincide with the characteristic mechanical impedances of the plate.

For cases where the support is viscoelastic, perfect absorption cannot be achieved, but absolute minima were identified in the reflection factors. The stiffness that minimized the vibration response of finite rectangular plates subject to distributed random excitations was calculated. The vibration of the compliantly supported rectangular plate was analyzed using the Rayleigh–Ritz method. The optimal stiffness values calculated from two different criteria (maximum dissipation of incident waves and minimum forced vibration response) were in good agreements.

The optimal translational stiffness for minimal radiated sound power was also calculated. It was found that this optimal translational stiffness is smaller than the values for minimal velocity response due to the increase in the number of radiating wave number components as the translational stiffness is increased. Similar numerical procedures can be applied to investigate the effects of rotational stiffness on the radiated sound power.

The modal response was found to be strongly regulated by the energy dissipation at the edges, which determined the amplitudes of the spatially averaged vibration response and the radiated sound power. In the cases of the window sealing system shown in this paper, the proposed methods to calculate the optimal support stiffness may be used as a guide in designing the geometry and the mechanical properties of vehicle window seals. The support stiffness that minimizes the reflection at the edges may be used as a first cut estimate for tuning purposes.

Acknowledgements

The authors express their thanks to Ford Motor Company and Advanced Elastomer Systems for their financial support and their guidance throughout this project. The technical assistance of the Herrick Laboratories staff is also gratefully acknowledged.

Appendix A. Nomenclature

a, b	plate dimensions in x and y directions (m)
$\hat{A}, \hat{B}, \hat{C}$	complex amplitude of bending waves (m)
b_r	viscous rotational damper coefficients (N · s/rad)
b_t	viscous translational damper coefficients (Pa · s)
c	speed of sound in air (m/s)
D	bending stiffness of plate (N · m)
E	elastic modulus of plate (Pa)
f	frequency (Hz)
G_{pp}	wall pressure cross-spectral density (Pa^2/Hz)
h	plate thickness (m)
$\hat{H}_j$	frequency response functions in terms of generalized co-ordinates
k_a, k_b	wave number (rad/m)
M_{xx}	bending moment (N · m)
$n(f)$	modal density in cycles per second
N	degree of freedom
Q_{xz}	shear force (N)
$\mathbf{r}_1, \mathbf{r}_2, \mathbf{s}_1, \mathbf{s}_2$	position vectors on plate surface
R, T	non-dimensional stiffness parameters
$\hat{S}_r$	complex rotational stiffness of boundary support (N/rad)
$\hat{S}_t$	complex translational stiffness of boundary support (Pa)
$S_{t,opt}$	optimal real stiffness of translational spring (Pa)
v_{av}	spatially averaged mean square velocity of plate (m^2/s^2/Hz)
v_{ref}	reference mean square velocity, 10^{-12} m^2/s^2
v_{ω_0}	spatially averaged mean square velocity in octave bands (m^2/s^2)
$\hat{V}_j$	jth eigenvector of plate
w	transverse displacement of plate (m)
W_r	radiated sound power (W/Hz)

W_{ref}	reference power, 10^{-12} W
W_{ω_0}	radiated sound power in octave bands (W)
$\hat{\Psi}_{mn}$	modal shape functions of plate
η_j	system loss factor of jth mode
η_r, η_t	loss factors of rotational and translational spring
ρ_a, ρ_b	density of air and plate material, respectively (kg/m^3)
σ_j	radiation efficiency of jth mode
v	the Poisson ratio of plate
φ_x	angular deflection (rad)
Φ_p	pressure spectral density (Pa^2/Hz)
ω	circular frequency (rad/s)
ω_{nj}	damped natural frequency of jth mode (rad/s)
$\hat{\omega}_j$	complex natural frequency of jth mode (rad/s)
Indices	m, n, j integer

References

[1] J.C. Snowdon, Vibration and Shock in Damped Mechanical Systems, Wiley, New York, 1968.
[2] W. Soedel, Vibrations of Shells and Plates, Marcel Dekker, New York, 1993.
[3] K.-H. Kang, K.-J. Kim, Modal properties of beams and plates on resilient supports with rotational and translational complex stiffness, Journal of Sound and Vibration 190 (1996) 207–220.
[4] J.C. Macbain, J. Genin, Energy dissipation of a vibrating Timoshenko beam considering support and material damping, International Journal of Mechanical Science 17 (1975) 255–265.
[5] G. Chen, J. Zhou, Vibration and Damping in Distributed Systems, Volume II: WKB and Wave Methods, Visualization and Experimentation, CRC Press, Boca Raton, FL, 1993.
[6] J. Park, T. Siegmund, L. Mongeau, Analysis of the flow-induced vibrations of viscoelastically supported rectangular plates, Journal of Sound and Vibration 261 (2003) 225–245.
[7] F. Fahy, Sound and Structural Vibration: Radiation, Transmission and Response, Academic Press, London, 1985.
[8] S.S. Rao, Engineering Optimization, Wiley, New York, 1996.
[9] J.D. Ferry, Viscoelastic Properties of Polymers, Wiley, New York, 1980.
[10] D.E. Newland, An Introduction to Random Vibrations, Spectral & Wavelet Analysis, Addison Wesley Longman, Essex, UK, 1993.
[11] A. Berry, J.-L. Guyader, J. Nicolas, Ageneral formulation for the sound radiation from rectangular, baffled plates with arbitrary boundary conditions, Journal of the Acoustical Society of America 88 (1990) 2792–2802.
[12] C.E. Wallace, Radiation resistance of a rectangular panel, Journal of the Acoustical Society of America 51 (1972) 946–952.
[13] R.H. Lyon, R.G. Dejong, Theory and Application of Statistical Energy Analysis, Butterworth-Heinemann, Newton, MA, 1995.